The Benefit of Accelerometers Based on Cold Atom Interferometry for Future Satellite Gravity Missions

Annike Knabe ⓘ, Manuel Schilling ⓘ, Hu Wu ⓘ, Alireza HosseiniArani ⓘ, Jürgen Müller ⓘ, Quentin Beaufils ⓘ, and Franck Pereira dos Santos ⓘ

Abstract

Satellite gravity missions, like GRACE and GRACE Follow-On, successfully map the Earth's gravity field and its change over time. With the addition of the laser ranging interferometer (LRI) to GRACE-FO, a significant improvement over GRACE for inter-satellite ranging was achieved. One of the limiting factors is the accelerometer for measuring the non-gravitational forces acting on the satellite. The classical electrostatic accelerometers are affected by a drift at low frequencies. This drawback can be counterbalanced by adding an accelerometer based on cold atom interferometry (CAI) due to its high long-term stability. The CAI concept has already been successfully demonstrated in ground experiments and is expected to show an even higher sensitivity in space.

In order to investigate the potential of the CAI concept for future satellite gravity missions, a closed-loop simulation is performed in the context of GRACE-FO like missions. The sensitivity of the CAI accelerometer is estimated based on state-of-the-art ground sensors and predictions for space applications. The sensor performance is tested for different scenarios and the benefits to the gravity field solutions are quantitatively evaluated. It is shown that a classical accelerometer aided by CAI technology improves the results of the gravity field recovery especially in reducing the striping effects. The non-gravitational accelerations are modelled using a detailed surface model of a GRACE-like satellite body. This is required for a realistic determination of the variations of the non-gravitational accelerations during one interferometer cycle. It is demonstrated that the estimated error due to this variation is significant. We consider different orbit altitudes and also analyze the effect of drag compensation.

A. Knabe (✉) · H. Wu · A. HosseiniArani · J. Müller
Institut für Erdmessung, Leibniz Universität Hannover, Hannover, Germany
e-mail: knabe@ife.uni-hannover.de

M. Schilling
Institut für Satellitengeodäsie und Inertialsensorik, Deutsches Zentrum für Luft- und Raumfahrt e.V. (DLR), Hannover, Germany

Q. Beaufils · F. Pereira dos Santos
LNE-SYRTE, Observatoire de Paris-PSL Université, CNRS, Sorbonne Université, Paris, France

1 Introduction

The Earth's gravity field and its variation are of great interest for several disciplines (Pail et al. 2015). The measurement of the time-variable gravity field, i.e. monitoring of mass variations, was successfully realized by the satellite mission GRACE (Tapley et al. 2019) and is now continued by GRACE Follow-On (Landerer et al. 2020). The limiting factor on the instrument level is the accelerometer.

It is needed to measure the non-gravitational accelerations acting on the satellite which are subtracted in the post-processing to retrieve the Earth's gravity field information. In the current satellite missions, electrostatic accelerometers are used. These sensors are characterized by their low noise at the high frequencies. The main drawbacks of electrostatic accelerometers are the drift at the low frequencies and the difficulty in the estimation of biases and scale factors.

The technology of Cold Atom Interferometry (CAI) could solve these challenges. A cloud of independent cold atoms constitute the test mass in an atom interferometer. The benefit of atom interferometry accelerometers is their high long-term stability and good knowledge of the scale factor which is based on the frequency stability of the laser system. Simulation studies like Abrykosov et al. (2019) and Müller and Wu (2020) show promising improvements by CAI for the gravity field recovery. In Fig. 1, the noise behaviour of the accelerometer types are displayed in terms of Amplitude Spectral Density (ASD), which is defined as the square root of the Power Spectral Density (PSD). The hybrid sensor is a combination of an atomic interferometer and an electrostatic accelerometer. The performances for CAI are based on the anticipation of a large interrogation time in microgravity. In this contribution, a closed-loop simulation is performed to study the benefit of CAI accelerometry. The sensitivity of the measurements increases with higher interaction time. As the satellite is moving during the measurements, the non-gravitational acceleration varies in one interferometer cycle. In this study we use a cycle time (duration of one CAI measurement) of 12 s and evaluate the variation of the acceleration using the transfer function of an atomic interferometer.
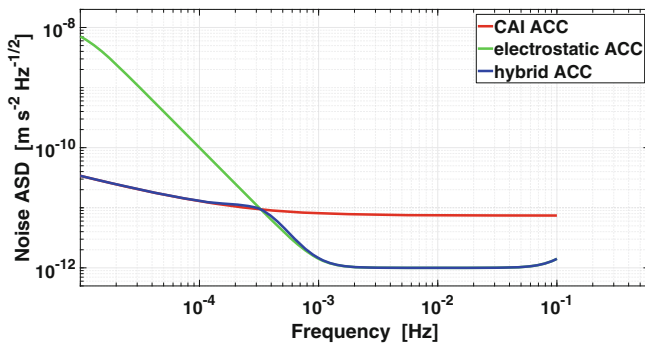

Fig. 1 Anticipated ASD of a space accelerometer noise: CAI accelerometer, electrostatic accelerometer and hybrid accelerometer

2 Performance of an Atom Interferometry Accelerometer

In an atom interferometer, cold atoms are in free fall and operate as test mass. Laser pulses in a time interval T are used to split and recombine the atomic wave functions into different momentum states according to the superposition principle (Pereira dos Santos and Landragin 2007; Schilling et al. 2012). The output phase Φ can be obtained by measuring the relative atomic populations in the output states after recombination. The acceleration a_k during cycle k is obtained from the measured phase Φ_k with the evolution time T:

$$a_k = \frac{\Phi_k}{k_{eff} T^2}, \tag{1}$$

where $k_{eff} = |\mathbf{k}_{eff}|$ is the norm of the effective wave vector of the laser light used to transfer momentum to the atoms (Kasevich and Chu 1991). In this study, the duration of one interferometer measurement cycle T_c is 12 s. It consists of the preparation time T_p, the interferometer duration $2T$ and the detection time T_d:

$$T_c = T_p + 2T + T_d. \tag{2}$$

As the sensitivity of the accelerometer to the acceleration varies during one measurement cycle, the transfer function must be taken into account. The phase of the interferometer Φ_k at the k-th cycle is given by

$$\Phi_k = k_{eff} \int_{kT_c}^{(k+1)T_c} g_{a,k}(t)a(t)dt. \tag{3}$$

The response function $g_{a,k}$ (see Fig. 2) is given by

$$g_{a,k}(t) = 0 \quad \text{for } kT_c < t < kT_c + T_p,$$

$$g_{a,k}(t) = t - (kT_c + T_p)$$
$$\qquad \text{for } kT_c + T_p < t < kT_c + T_p + T,$$

$$g_{a,k}(t) = kT_c + T_p + 2T - t$$
$$\qquad \text{for } kT_c + T_p + T < t < kT_c + T_p + 2T,$$

$$g_{a,k}(t) = 0 \quad \text{for } kT_c + T_p + 2T < t < (k+1)T_c.$$

To estimate the performance, we used parameters based on state of the art accelerometers on ground. The number of interfering atoms is $N = 10^6$ and the contrast is $C = 0.8$. The momentum transfer, depending on laser wavelength λ,
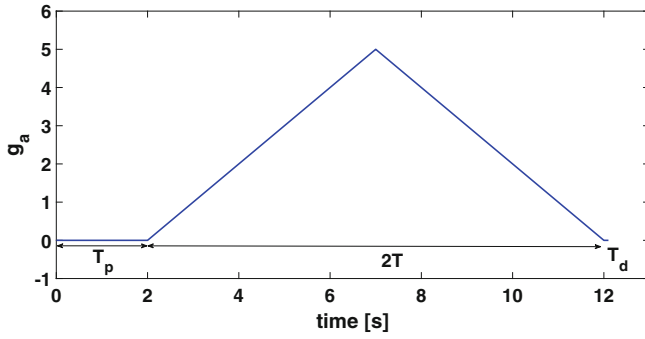
Fig. 2 Response in the time domain of the transfer function for the conversion of the phase shift to acceleration

Fig. 3 Anticipated ASD of a space CAI accelerometer noise

is $k_{eff} = 4\pi\lambda \approx 1.6 \times 10^7$ /m for a two photon Raman transition using rubidium atoms. Microgravity in space is expected to allow for a dramatic increase of the free fall interferometer interrogation time T, which would greatly improve the performances of a CAI. For the following calculations we consider a measurement time of $T = 5$ s and a preparation time of 2 s. The detection time is neglected as it is only a few tens of ms.

The quantum projection limited phase noise is given by

$$\sigma_\Phi = \sqrt{\frac{T_c}{C^2 N}} = 4.2 \text{ mrad}/\sqrt{\text{Hz}}. \tag{4}$$

The sensitivity function of a 3 pulse atom interferometer is

$$H(f) = 16 \frac{(2k_{eff})^2}{(2\pi f)^4} \sin^4(2\pi f T/2). \tag{5}$$

In order to take into account fluctuations of systematic effects, we impose a $1/f$ flicker floor noise of $\sigma_f = 0.1$ mrad. The acceleration PSD can then be expressed as (see Fig. 3)

$$S_a^2(f) = (2\sigma_\Phi^2 + 2 \ln(2)\sigma_f^2/f)/H(f). \tag{6}$$

We use this model in the following to estimate the performances of a CAI accelerometer in a satellite.

3 Variation of Non-Gravitational Accelerations Within One Interferometer Cycle

Time series of the non-gravitational accelerations are simulated with the Extended High Performance Satellite Dynamics Simulator (XHPS) Software (Wöske et al. 2016) developed by ZARM/DLR. Models for atmospheric drag and solar radiation pressure, Earth albedo, thermal radiation pressure and infrared are included in the simulations. In
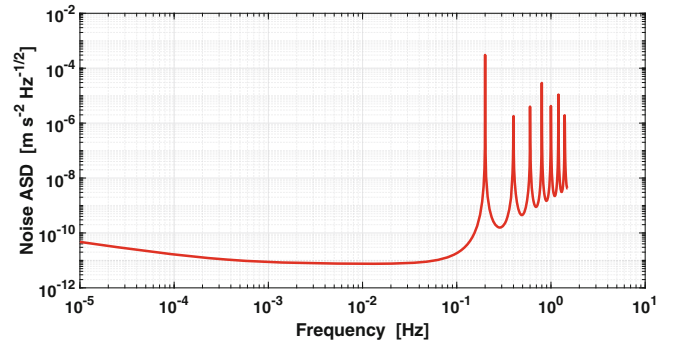
this study, only accelerations in the along-track direction are included, because in this direction the magnitude of the non-gravitational accelerations is the biggest and consequently the biggest effect is expected here. In this section, only a single satellite is investigated. An attitude control system with a nadir pointing mode is included in the calculation of the non-gravitational accelerations. Misalignment errors and errors due to the non-orthogonality of the accelerometer frame axes are not considered in this study. Degradation induced by the cross-track and nadir axes would appear when the true alignment differs from the target alignment. Two simulations are investigated with satellite altitudes of 467 km and 303 km. The satellite's mass is assumed to be equal to 600.98 kg. A detailed surface model of a GRACE-like satellite body is used. The mass and shape of the satellite and the altitude of 467 km are the parameters of the GRACE-FO mission, allowing a realistic comparison to the results of the mission. In addition, a lower altitude of 303 km is chosen, which would lead to a higher sensitivity to the gravity field signal at the cost of higher non-gravitational accelerations and is thus interesting for future gravity missions. In order to get a continuous signal for the computation of ϕ_k in Eq. (3), the acceleration time series is approximated with an interpolation polynomial. The Newton polynomial interpolation is applied for each cycle separately. The best agreement is achieved with a quadratic polynomial. The variation between the minimum acceleration and the maximum acceleration within one cycle is calculated for the two satellite orbits (Fig. 4). The variation in 12 s is of the order of 10^{-9} m/s^2 for an altitude of 467 km and 10^{-8} m/s^2 for an altitude of 303 km. This variation is higher than the accelerometer noise itself (Fig. 1).

The transfer function of an atomic interferometer is used to investigate the effect of this variation in one cycle. The output of the atom interferometer is compared to the true acceleration value at $t = 7$ s of each cycle, i.e. the middle time of the interferometer. In Fig. 5 the ASD of this difference and the ASD of the variation in one cycle are shown. The estimated error of the acceleration measurements is at the level of
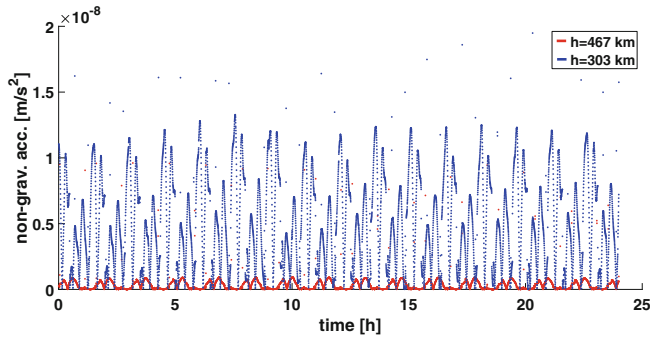
Fig. 4 Variation of non-gravitational accelerations within one interferometer cycle for two different altitudes: 467 km (red) and 303 km (blue)
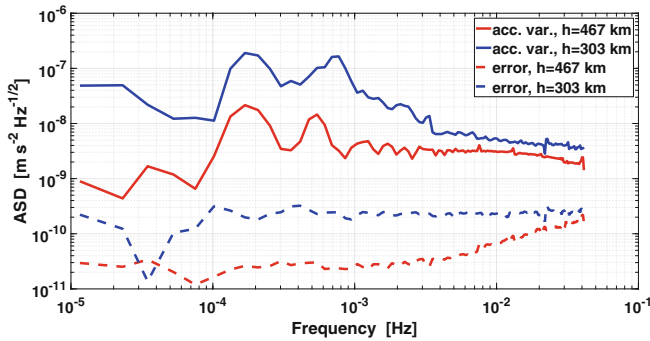

Fig. 5 ASD of variation of non-gravitational accelerations within one interferometer cycle (acc. var.) and corresponding error contribution to the CAI measurements (error) for two different altitudes: 467 km and 303 km

Fig. 6 Residual variation of non-gravitational accelerations within one interferometer cycle under drag free control

Fig. 7 ASD of residual variation of non-gravitational accelerations within one interferometer cycle and corresponding error contribution under drag free control

3×10^{-11} m/s^2 for an altitude of 467 km and 2×10^{-10} m/s^2 for an altitude of 303 km. In comparison to the acceleration noise this error contribution is significant, which shows that one needs to take into account the temporal filtering of non-inertial accelerations due to the interferometer response function.

Furthermore, the impact of using a drag compensation system is studied. The thruster is modelled with parameters of the GOCE mission. The thruster noise is simulated using a PSD model (Canuto et al. 2010):

$$S_{thr}^2(f) = \left(\left(\frac{0.005}{f} \right)^2 + 1 \right) \left(10^{-6} \right)^2 \ \text{N}^2/\text{Hz}. \quad (7)$$

For the thruster system a maximum thrust level of 21 mN, a minimum thrust level of 0.6 mN and a possible rate of change of 2.5 mN/s are considered. As it is impossible to find a good fitting polynomial for the time series including thruster noise, a filter is first applied. A second order Butterworth filter with cutoff frequencies of 1×10^{-6} Hz and 5×10^{-3} Hz is used. The variation of accelerations within one interferometer cycle is shown in Fig. 6 and its ASD in Fig. 7. The estimated error contribution due to the residual variation of
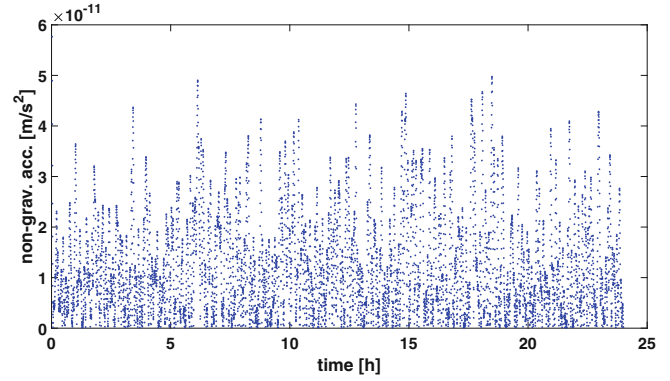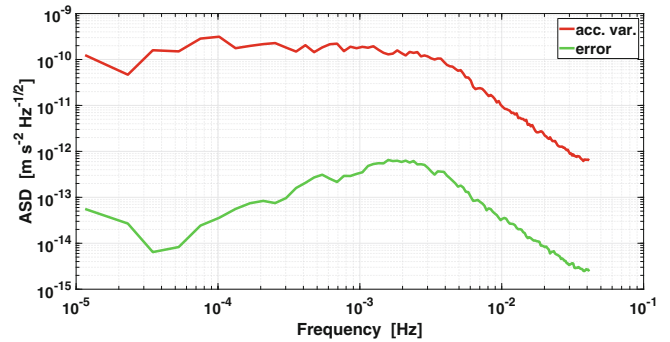
non-gravitational accelerations is now below the noise of an atomic interferometer and hence acceptable (Fig. 7). In summary, the acceleration variation in one interferometer cycle has to be taken into account because it can have a critical impact on the performance of the CAI accelerometer. A balance between the cycle time length and sensitivity has to be found. Drag compensation is a good option to reduce the impact of this acceleration variation.

4   Closed-Loop Simulation

4.1   Simulation Procedure

A closed-loop simulation of a GRACE-FO like mission is performed to investigate the potential of the combination of an electrostatic and a CAI accelerometer. Figure 8 shows the flowchart of the simulation procedure. It consists of the synthesis of range accelerations based on the input satellite orbit and the gravity field model, addition of instrument noise and model errors and the gravity field recovery. The reference gravity field model is only a static model which means no temporal gravity field signals are included, since
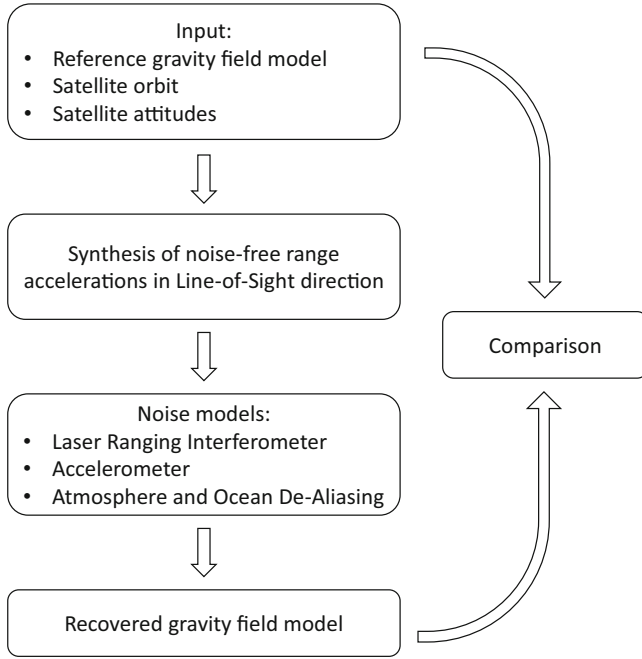
Fig. 8 Flowchart of the closed-loop simulation

Fig. 9 ASD of the different noise sources

the main purpose of this study is to evaluate the contributions of CAI accelerometer w.r.t. the electrostatic one. In order to recover the temporal gravity fields, in a future study we will use a sequence of monthly simulated data which includes not only the static model but also the temporal signals. Ocean tide errors and non-tidal gravity field signals are not included, but an error due to Atmosphere and Ocean Aliasing is considered. We know that some ocean tide components might cause aliasing effects on recovered solutions. But as a preliminary study, we suppose that the ocean tides and direct tides can be precisely modelled and reduced from the observations. The range accelerations in Line-of-Sight direction $\ddot{\rho}$, measured by the Laser Ranging Interferometer (LRI), are synthesized with:

$$\ddot{\rho} = \ddot{\boldsymbol{r}}_{AB}\,\boldsymbol{e}_{AB} + \dot{\boldsymbol{r}}_{AB}\,\dot{\boldsymbol{e}}_{AB}, \tag{8}$$

where $\ddot{\boldsymbol{r}}_{AB} = \ddot{\boldsymbol{r}}_B - \ddot{\boldsymbol{r}}_A$ is the difference of the gradient of the Earth's gravitational potential at the positions of the two satellites A and B, $\boldsymbol{e}_{AB}$ is the unit vector of the Line-of-Sight and $\dot{\boldsymbol{e}}_{AB}$ is its derivative, $\dot{\boldsymbol{r}}_{AB} = \dot{\boldsymbol{r}}_B - \dot{\boldsymbol{r}}_A$ is the velocity difference between satellites A and B. The second term $\dot{\boldsymbol{r}}_{AB}\,\dot{\boldsymbol{e}}_{AB}$ is neglected in this study because no acceleration measurements for its estimation are needed and the focus is put on the benefit of novel accelerometers. The magnitude of this term is estimated to be lower than 4.3×10^{-9} m/s^2 for a GRACE-like mission scenario. In the next step, noise models for different error sources are added: LRI measurement noise, accelerometer noise and Atmospheric and Ocean
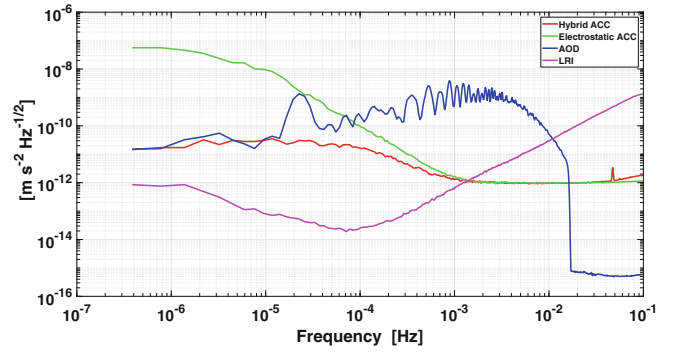
De-Aliasing noise (AOD). The LRI noise is modelled according to Abich et al. (2019). The Atmospheric and Ocean De-Aliasing models errors are assumed as 10% of AOD1B RL6 (Dobslaw et al. 2017). The ASD of these noise contributions is shown in Fig. 9. The spherical harmonic coefficients S_{nm} and C_{nm} are estimated with a least-squares adjustment. The observation equation of the adjustment is linear as the range accelerations provide a direct link to the gravity field coefficients. The gravity field model is solved up to degree and order 90. The reference gravity field model is Eigen-6c4 (Foerste et al. 2014) and the GRACE orbit from April 2006 is used. A perfect alignment of each satellite is assumed so that the non-gravitational accelerations can be measured with accuracy by the 1-axis hybrid accelerometer in this study. The variance-covariance matrix, which is assembled from the post-fit residuals, is used for the stochastic modelling.

4.2 Simulation Results

For the evaluation the differences between the input reference gravity field model and the recovered gravity field model are calculated. The coefficient differences of gravity fields recovered applying different types of accelerometers are then compared. The evaluation is carried out in the spectral and the space domain. The equivalent water height (EWH) is calculated to validate the results in the space domain using the following equation (Schrama et al. 2007; Wahr et al. 1998):

$$\Delta EWH = \frac{R\,\rho_e}{3\rho_w} \sum_{n=0}^{N} \frac{2n+1}{1+k_n} \sum_{m=0}^{n} (\Delta C_{nm} \cos(m\lambda) \\ + \Delta S_{nm} \sin(m\lambda))\, P_{nm}(\cos(\Theta)), \tag{9}$$

where R is the radius of the Earth, ρ_e is the average density of the Earth, ρ_w is the density of water, k_n is Love number of degree n, λ is the longitude and Θ the polar distance.
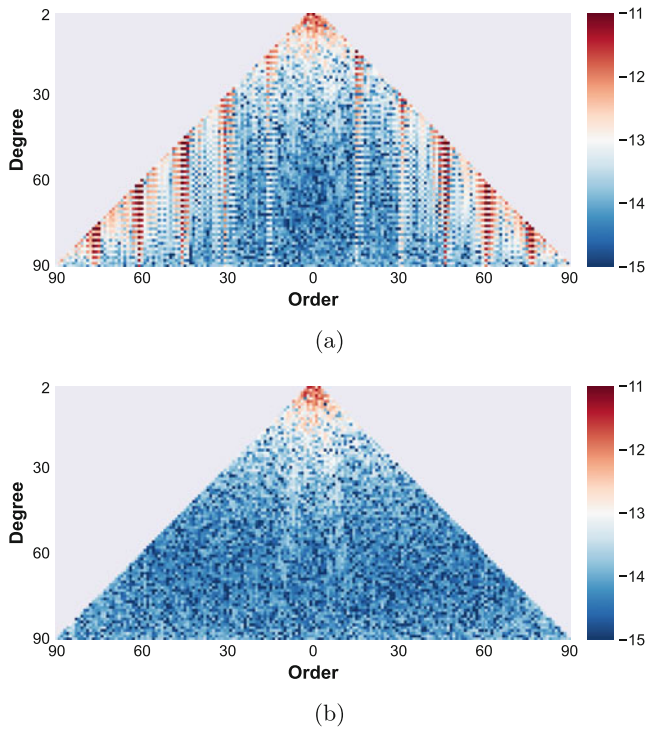
(a)

(b)

Fig. 10 Coefficient differences between recovered and reference gravity field using in the closed-loop simulation the noise model of (a) an electrostatic accelerometer and (b) a hybrid accelerometer
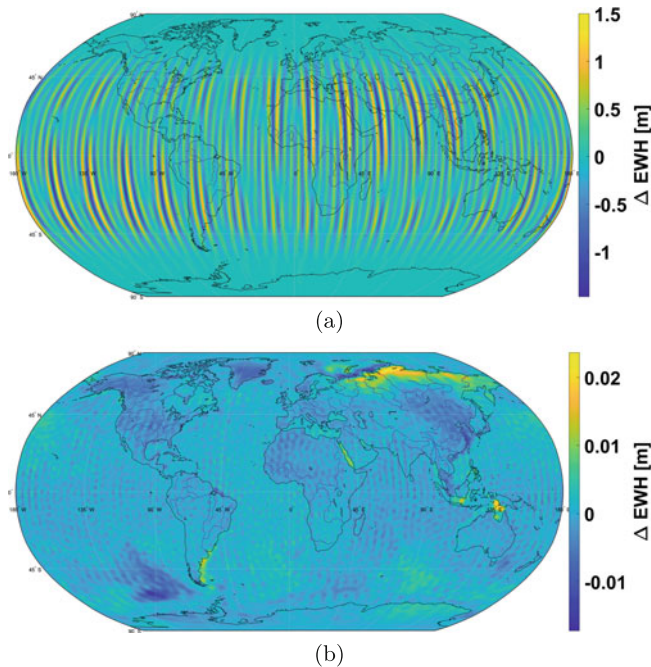

(a)

(b)

Fig. 11 Coefficient differences between recovered and reference gravity field expressed in terms of equivalent water height using in the closed-loop simulation the noise model of (a) an electrostatic accelerometer and (b) a hybrid accelerometer

ΔC_{nm} and ΔS_{nm} are the coefficient differences and P_{nm} are the Legendre functions.

In Fig. 10, the true errors are represented as two-dimensional spectrum. The result with the electrostatic accelerometer shows large striping effects at orders $m = 16 \times k, k \in \mathbb{N}$. These specific orders correspond to the orbit frequency and multiples of it. This reveals, that the CAI accelerometer counteracts the problem with orbit resonances and striping effects owing to its low noise in the low frequencies. It can be concluded that the bias drift of the electrostatic accelerometer in the low frequencies causes degradation in the orbital resonance order 16 and integer multiples of it. However, this problem can also be solved by filtering because the frequencies below 1.8×10^{-4} Hz imply no gravity field signal. In McGirr et al. (2022), an improvement of the GRACE gravity solutions is achieved by applying a high-pass filter to the accelerometer data and removing the low-frequency components below 4.5×10^{-5} Hz.

The evaluation of the true errors in the spatial domain confirms a great improvement of the recovered gravity field for the simulation with a hybrid accelerometer. The striping effects using an electrostatic accelerometer are also visible in the space domain (Fig. 11). The striping effects in North-South direction are caused by the sampling and flight direction of the in-line pair. These systematic effects are characteristic for the GRACE solution. That is why, typically a filter is applied to the solutions. The stripes in the space domain are largely reduced by the combination with the CAI accelerometer. The errors expressed as EWH are two orders of magnitude lower when using the hybrid sensor. In Fig. 11b, the dominant factor is the AOD error. This can be observed by comparing the coefficient differences to the input AOD noise. The solution using an electrostatic accelerometer is also degraded by the AOD noise.

According to Abrykosov et al. (2019) the accelerometer noise is not the limiting factor when considering all non-tidal temporal signals. It must be noted that several assumptions are applied in our study. Some contributors to the error budget due to temporal variations are not considered. One example is the ocean tide aliasing which is one of the limiting factors. For a more realistic investigation, further signals and errors have to be included in upcoming studies.

5 Conclusions

The performance of an atom interferometry accelerometer is estimated based on state of the art atomic accelerometers on ground and various predicted space scenarios. The decisive advantage of the CAI sensor is its high long-term stability.

The variation of accelerations within one interferometer cycle is analysed using the transfer function of an atomic interferometer. For both simulations with altitudes of 303 km and 467 km the corresponding error is bigger

than the anticipated CAI noise. It means, this aspect is significant and must be considered for future gravity field missions. Consequently, a possible reduction of this effect when using a drag compensation system is studied. The simulation including drag compensation shows a reduced error contribution which is below the anticipated noise level of the atom interferometer.

A closed-loop simulation is performed to investigate the benefit of the CAI sensor for the recovered gravity field. The gravity field solution shows an improvement by a factor of two when using a hybridization of a CAI accelerometer and a classical electrostatic accelerometer. In the space domain, the striping effect is largely reduced. Accordingly, frequencies below 1×10^{-4} Hz have an influence on the gravity solutions, which can be justified by the bias drift of the accelerometer. Nevertheless, the signal below this frequency could also be removed by filtering without affecting the gravity field solution. The coefficient differences between recovered and reference gravity field indicate the input AOD error. This is especially visible when using a hybrid accelerometer and shows that the aliasing effects are the limiting factor. However, it has to be noted that not all temporal signals are included in our simulation and their effect to the gravity field solution might be even bigger.

Conflict of Interest

The authors declare that they have no conflict of interest.

Author Contributions Q.B. and F.P.d.S. provided input for the performance of the atom interferometer. H.W., M.S. and A.K. developed the software. A.K. performed the computations and wrote the first draft of the manuscript. All authors provided critical input to the manuscript and approved the final version.

Data Availability Statement Datasets generated in this study are available from the corresponding author on reasonable request.

References

Abich K, Abramovici A, Amparan B, Baatzsch A, Okihiro BB, Barr DC, Bize MP, Bogan C, Braxmaier C, Burke MJ, Clark KC, Dahl C, Dahl K, Danzmann K, Davis MA, de Vine G, Dickson JA, Dubovitsky S, Eckardt A, Ester T, Barranco GF, Flatscher R, Flechtner F, Folkner WM, Francis S, Gilbert MS, Gilles F, Gohlke M, Grossard N, Guenther B, Hager P, Hauden J, Heine F, Heinzel G, Herding M, Hinz M, Howell J, Katsumura M, Kaufer M, Klipstein W, Koch A, Kruger M, Larsen K, Lebeda A, Lebeda A, Leikert T, Liebe CC, Liu J, Lobmeyer L, Mahrdt C, Mangoldt T, McKenzie K, Misfeldt M, Morton PR, Müller V, Murray AT, Nguyen DJ, Nicklaus K, Pierce R, Ravich JA, Reavis G, Reiche J, Sanjuan J, Schütze D, Seiter C, Shaddock D, Sheard B, Sileo M, Spero R, Spiers G, Stede G, Stephens M, Sutton A, Trinh J, Voss K, Wang D, Wang RT, Ware B, Wegener H, Windisch S, Woodruff C, Zender B, Zimmermann M (2019) In-orbit performance of the GRACE follow-on laser ranging interferometer. Phy Rev Lett 123(3):031101. https://doi.org/10.1103/PhysRevLett.123.031101

Abrykosov P, Pail R, Gruber T, Zahzam N, Bresson A, Hardy E, Christophe B, Bidel Y, Carraz O, Siemes C (2019) Impact of a novel hybrid accelerometer on satellite gravimetry performance. Adv Space Res 63(10):3235–3248. https://doi.org/10.1016/j.asr.2019.01.034

Canuto E, Molano A, Massotti L (2010) Drag-free control of the GOCE satellite: Noise and observer design. IEEE T Contr Syst T 18(2):501–509. https://doi.org/10.1109/TCST.2009.2020169

Dobslaw H, Bergmann-Wolf I, Dill R, Poropat L, Thomas M, Dahle C, Esselborn S, König R, Flechtner F (2017) A new high-resolution model of non-tidal atmosphere and ocean mass variability for de-aliasing of satellite gravity observations: AOD1B RL06. Geophys J Int 211(1):263–269. https://doi.org/10.1093/gji/ggx302

Foerste C, Bruinsma S, Abrykosov O, Lemoine JM, Marty JC, Flechtner F, Balmino F Gand Barthelmes, Biancale R (2014) EIGEN-6C4 The latest combined global gravity field model including GOCE data up to degree and order 2190 of GFZ Potsdam and GRGS Toulouse. GFZ data services 10. https://doi.org/10.5880/icgem.2015.1

Kasevich M, Chu S (1991) Atomic interferometry using stimulated Raman transitions. Phy Rev Lett 67(2):181–184. https://doi.org/10.1103/PhysRevLett.67.181

Landerer FW, Flechtner FM, Save H, Webb FH, Bandikova T, Bertiger WI, Bettadpur SV, Byun SH, Dahle C, Dobslaw H, Fahnestock E, Harvey N, Kang Z, Kruizinga GLH, Loomis BD, McCullough C, Murböck M, Nagel P, Paik M, Pie N, Poole S, Strekalov D, Tamisiea ME, Wang F, Watkins MM, Wen HY, Wiese DN, Yuan DN (2020) Extending the global mass change data record: GRACE Follow-On instrument and science data performance. Geophys Res Lett 47(12):e88306. https://doi.org/10.1029/2020GL088306

McGirr R, Tregoning P, Allgeyer S, McQueen H, Purcell A (2022) Mitigation of thermal noise in GRACE accelerometer observations. Adv Space Res 69(1):386–401. https://doi.org/10.1016/j.asr.2021.10.055

Müller J, Wu H (2020) Using quantum optical sensors for determining the Earth's gravity field from space. J Geod 94(8):1–14. https://doi.org/10.1007/s00190-020-01401-8

Pail R, Bingham R, Braitenberg C, Dobslaw H, Eicker A, Güntner A, Horwath M, Ivins E, Longuevergne L, Panet I, et al. (2015) Science and user needs for observing global mass transport to understand global change and to benefit society. Surv Geophys 36(6):743–772. https://doi.org/10.1007/s10712-015-9348-9

Pereira dos Santos F, Landragin A (2007) Getting the measure of atom interferometry. Phys World 20(11):32–37. https://doi.org/10.1088/2058-7058/20/11/38

Schilling M, Timmen L, Müller J (2012) Einsatz der Atominterferometrie in der Geodäsie. zfv 137(3/2012):185–194. https://doi.org/10.15488/3097

Schrama EJO, Wouters B, Lavallée DA (2007) Signal and noise in Gravity Recovery And Climate Experiment (GRACE) observed surface mass variations. J Geophys Res 112(B08407). https://doi.org/10.1029/2006JB004882

Tapley BD, Watkins MM, Flechtner F, Reigber C, Bettadpur S, Rodell M, Sasgen I, Famiglietti JS, Landerer FW, Chambers DP, Reager JT, Gardner AS, Save H, Ivins ER, Swenson SC, Boening C, Dahle C, Wiese DN, Dobslaw H, Tamisiea ME, Velicogna I (2019) Contributions of GRACE to understanding climate change. Nat Clim Change 9:358–369. https://doi.org/10.1038/s41558-019-0456-2

Wahr J, Molenaar M, Bryan F (1998) Time variability of the Earth's gravity field: Hydrological and oceanic effects and their possible detection using GRACE. J Geophys Res 103(B12):30205–30229. https://doi.org/10.1029/98JB02844

Wöske F, Kato T, List M, Rievers B (2016) Development of a high precision simulation tool for gravity recovery missions like GRACE. In: Zanetti R, Russel RP, Ozimek MT, Bowes AL (eds) Proceedings of the 26th AAS/AIAA space flight mechanics meeting held February 14–18, 2016. Advances in the Astronautical Sciences, vol 158, pp 2445–2457